Study on the saturation characteristics of high-speed uni-traveling-carrier photodiodes based on field screening analysis

Tuo Shi (石 拓), Bing Xiong (熊 兵)*, Changzheng Sun (孙长征), and Yi Luo (罗 毅)

Tsinghua National Laboratory for Information Science and Technology, State Key Lab on Integrated Optoelectronics, Department of Electronic Engineering, Tsinghua University, Beijing 100084, China

Corresponding author: bxiong@tsinghua.edu.cn

Received February 28, 2011; accepted March 25, 2011; posted online May 31, 2011

A back-illuminated mesa-structure InGaAs/InP charge-compensated uni-traveling-carrier (UTC) photodiode (PD) is fabricated, and its saturation characteristics are investigated. The responsivity of the 40-μm-diameter PD is as high as 0.83 A/W, and the direct current (DC) saturation current is up to 275 mA. The 1-dB compression point at the 3-dB cutoff frequency of 9 GHz is measured to be 100 mA, corresponding to an output radio frequency (RF) power of up to 20.1 dBm. According to the calculated electric field distributions in the depleted region under both DC and alternating current (AC) conditions, the saturation of the UTC-PD is caused by complete field screening at high optical injection levels.

OCIS codes: 230.5170, 250.0040.

doi: 10.3788/COL201109.082302.

Analog optical links are favored for many microwave applications, such as phased array antennas and wireless-over-fiber systems, due to their advantages of low transmission loss, wide bandwidth, reduced size and weight, and immunity to electromagnetic interference[1−3]. To improve the performances of the analog links, such as link gain, noise figure, and spurious-free dynamic range (SFDR), one of the key issues that must be considered is utilizing photodiodes (PDs) possessing high quantum efficiency and the ability to handle high optical power, i.e., PDs with high responsivity and high saturation photocurrent[4]. Many studies have been undertaken to increase the responsivity, such as those on evanescently coupled photodiodes combined with multimode diluted waveguide[5] and three-mirror cavity photodetector[6]. Meanwhile, research on improving the saturation performance of PDs has attracted plenty of attention. Various device structures, such as uni-traveling-carrier (UTC)[7,8], partially depleted-absorber[9] and dual-depletion region[10], have been proposed to improve the bandwidth and saturation photocurrent of PDs by tailoring carrier traveling process in the depletion region. Moreover, optimizing the electric field in the depletion region can modulate the electron drift velocity, thus relieving the carrier pileup and increasing response speed[11,12]. Due to the carrier pileup in the depletion region under high current, space-charge effect, which causes the electric field redistribution, degrades the performance of a PD at high optical injection levels, leading to output radio frequency (RF) power compression, bandwidth reduction, and significant nonlinearity[13]. However, to the best of our knowledge, there have only been relatively few reports on the relationship between the electric field distribution and the estimation of PD saturation performance, which is crucial for applications requiring high output RF power.

In this letter, we report the fabrication and analysis of a high performance, modified UTC-PD designed for analog optical link applications. The UTC-PD exhibits responsivity of up to 0.83 A/W and a high direct current (DC) saturation current of 275 mA. The 1-dB compression point is 100 mA at the 3-dB cutoff frequency of 9 GHz, corresponding to a RF output power of as high as 20.1 dBm. The electric field distribution within the UTC-PD under the DC and alternating current (AC) conditions are calculated, and complete field screening is found to be the cause of the measured saturation performance of the device. This study makes it possible to estimate the saturation characteristics of PDs by analyzing the electric field distribution.

The epitaxial layer structure of our UTC-PD is shown in Fig. 1, which is similar to the one depicted in Ref. [14]. The intrinsic layers were lightly doped to provide a

p^+-$In_{0.53}Ga_{0.47}As$, (50 nm)
p^+-InP, (1,000 nm)
p-$In_{0.53}Ga_{0.47}As$, (650 nm)
n^--$In_{0.53}Ga_{0.47}As$, (200 nm)
InGaAsP,Q1.4, (15 nm)
InGaAsP,Q1.1, (15 nm)
n^--InP, (605 nm)
n^+-InP, (1,000 nm)
n^+-$In_{0.53}Ga_{0.47}As$, (20 nm)
n^+-InP buffer layer, (200 nm)
semi-insulate InP substrate

Fig. 1. Epitaxial layer structure of the modified UTC-PD.

 © 2011 Chinese Optics Letters

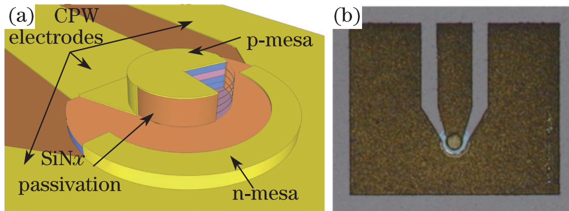

Fig. 2. (a) Schematic device structure and (b) top view image of the modified UTC-PD.

preplaced positive ion charge distribution that can mitigate the screening effect due to photogenerated electrons diffused into the depletion region. This type of charge compensation effectively adjusts the field distribution under high injection levels as well as increases the saturation current[15]. The device was grown on a semi-insulating InP substrate by metal organic chemical vapor deposition (MOCVD). An inductively coupled plasma (ICP) dry etching-based fabrication process was developed to complete the modified UTC-PD structure. First, in order to obtain optimum p-type ohmic contact, patterned Ti/Pt/Au p-type electrode was formed with a magnetron sputtering and lift-off process. To form the p-mesa structure, a 600-nm-thick SiN_x mask was deposited with plasma enhanced chemical vapor deposition (PECVD) to protect the electrode and the p-type ohmic contact layer on top of the mesa. Then, ICP dry-etching process was adopted to etch down to the n^+-InP collector layer, followed by a wet etching step using the InGaAs layer as etch stop. The sidewall of the p-mesa was then covered by a 300-nm-thick SiN_x for passivation. Patterned Ni/Au was then formed on the n^+-InGaAs layer for n-type ohmic contact, after which ICP dry etching was applied again to complete the n-mesa structure. Another 600-nm-thick SiN_x layer was deposited and patterned as low-k dielectric layer beneath the p- and n-electrodes. Coplanar waveguide structure was fabricated on top of the SiN_x layer for microwave signal transmission. The device electrode was then thickened by electroplating. Finally, the backside of the device was polished and anti-reflection coated with SiN_x film to improve the optical coupling efficiency. The resulting structure of the completed device is shown in Fig. 2.

One of the key techniques during the UTC-PD fabrication is the ICP dry etching process for mesa formation. Accurate control of the etching rate is important to guarantee the etching depth. Meanwhile, etched mesa with smooth and vertical sidewall is essential for desirable sidewall passivation. By adjusting the etching parameters, such as gas flow, RF power, and chamber pressure, it is possible to optimize the dip angle and the smoothness of the etched sidewall[16]. Non-concave vertical sidewall is realized by ICP dry etching using $Ar/Cl_2/CH_4$ gas mixture.

Backside polishing is another critical process for improving the optical coupling efficiency of the PD. For PDs with small absorption area, appropriate device backside thinning is necessary to achieve high optical coupling efficiency. The smoothness of the polished back surface was characterized with atomic force microscope, and a root-mean-square roughness of 5 nm was recorded.

The fiber-coupled responsivity versus photocurrent

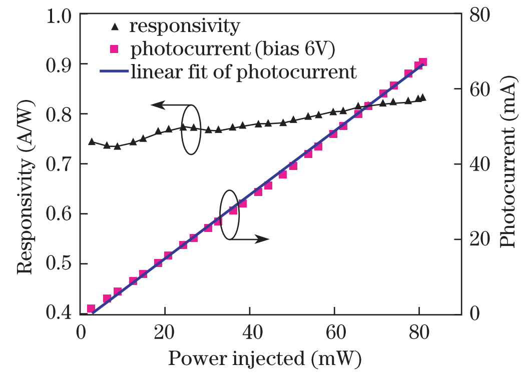

Fig. 3. Photocurrent and responsivity at different optical injection levels.

is shown in Fig. 3. At a reverse bias of 6 V, the responsivity at 1.55 μm was as high as 0.83 A/W. The dark current of a 40-μm diameter modified UTC-PD was measured to be about 2 μA for reverse bias at 8 V, which was about one order of magnitude larger than that reported[14]. This may be caused by the imperfect passivation of the mesa sidewall, and could be improved by optimizing the passivation process in the future.

The measured saturation performance under DC illumination is shown in Fig. 4(a). Saturation current under DC illumination of up to 275 mA was recorded. The electric field within the depletion region can be depicted by

$$V_{\mathrm{DC-Bias}} - I_{\mathrm{DC}} \cdot R_{\mathrm{s}} = \int E \mathrm{d}x, \tag{1}$$

$$\frac{\partial E}{\partial x} = \frac{q}{\varepsilon}(p - n + N_{\mathrm{D}} - N_{\mathrm{A}}), \tag{2}$$

where $V_{\mathrm{DC-Bias}}$ is the DC bias, I_{DC} is the DC photocurrent, R_{s} is the internal resistance, $N_{\mathrm{D}}(N_{\mathrm{A}})$ is the donor (acceptor) concentration, p (n) is the hole (electron)

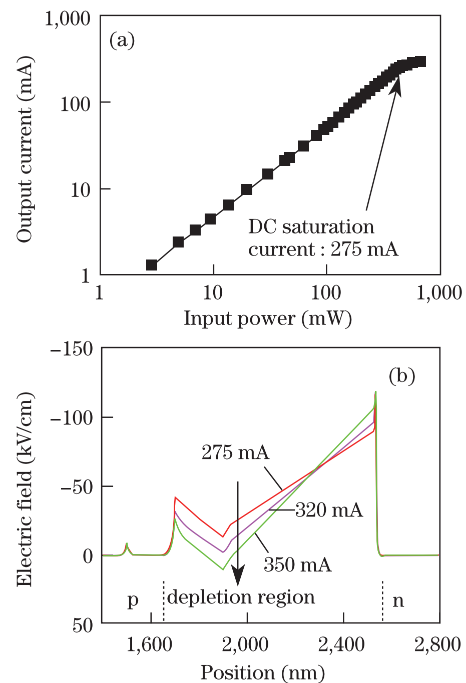

Fig. 4. (a) Saturation performance under DC illumination and (b) calculated electric field near saturation point.

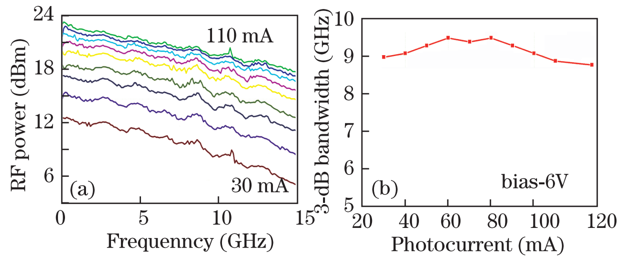

Fig. 5. (a) RF response and (b) 3-dB bandwidth of the modified UTC-PD under a reverse bias of 6 V.

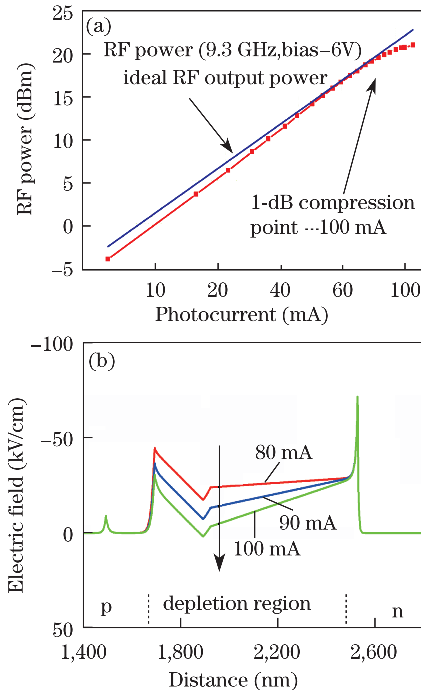

Fig. 6. (a) RF power delivered to a 50-Ω load for a 40-μm-diameter UTC-PD at 9.3 GHz and (b) calculated electric field around the 1-dB compression point.

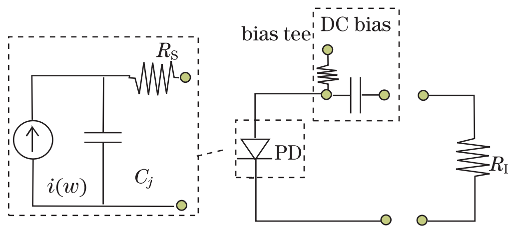

Fig. 7. Equivalent circuit of the RF response measurement setup.

concentration, and E is the electric field. These equations take into account the charge screening effect and voltage drop over the internal resistance under high power illumination. The calculated electric field under the DC current ranging from 275 to 350 mA is illustrated in Fig. 4(b). It can be seen that saturation occurrs when the electric field is completely screened by the drift electrons in the depleted region, which agrees well with our experimental results.

Frequency response and the output RF power of the UTC-PD were measured with 100% modulated light input generated through the two-laser heterodyne method[17]. The measured frequency responses and 3-dB bandwidths under different injection levels are plotted in Fig. 5. The 3-dB bandwidth of the diameter measuring 40 μm was found to be 9 GHz at a photocurrent of 100 mA. The capacitance and internal resistance derived from the measured S_{11} were about 0.3 pF and 10 Ω, respectively, indicating a 3-dB bandwidth of 8.8 GHz. This agrees well with our experimental results. The bandwidth of the PD can be further improved by decreasing the absorption area and optimizing the device structure, e.g., replacing the SiN_x insulation layer beneath the coplanar waveguide (CPW) electrodes with low dielectric constant materials, such as benzocyclobutene (BCB), to reduce the electrode capacitance.

Figure 6(a) shows the output RF power versus DC photocurrent at the frequency of 9.3 GHz, near the 3-dB bandwidth under a 6-V reverse bias. The measured 1-dB compression point was at the photocurrent of 100 mA, corresponding to an output RF power of 20.1 dBm. Apart from the charge screening effect and the voltage drop along the internal resistance, the load voltage swing induced by AC current delivered to the 50-Ω load also has significant influence on the AC saturation behavior[15]. Figure 7 shows the equivalent circuit of RF output power measurement system. From a circuital point of view, the actual voltage drop over the PD junction capacitance varies with the AC current, which can be described with Eqs. (3) and (4) represented by

$$\tilde{i} = i_0 + i_0 \mathrm{e}^{\mathrm{j}\omega t}, \quad (3)$$

$$V_{\mathrm{DC-Bias}} - \frac{R_{\mathrm{L}} i_0}{1 + \mathrm{j}\omega R_{\mathrm{L}} C} \mathrm{e}^{\mathrm{j}wt} - \tilde{i} \cdot R_{\mathrm{s}} = \int E \mathrm{d}x, \quad (4)$$

where $\tilde{i}$ is the AC photocurrent induced by light illumination of 100% modulation depth with the DC component of i_0 and the AC component of $i_0\mathrm{e}^{\mathrm{j}\omega t}$, R_{L} is the load resistance, and C is the PD junction capacitance. The saturation performance was determined by the lowest electric field distribution during an AC period, corresponding to the peak current point. For the DC component ranging from 80 to 100 mA, the calculated electric field is plotted in Fig. 6(b). From the results, It is clear that saturation occurrs when the electric field is completely screened by the drift electrons in the deleted range. Different from the DC case, the voltage which drops over the depeletion region is signifcantly affected by the voltage swing on the 50-Ω load, which results in lower saturation photocurrent.

From the above experimental measurement and theoretical analysis, the DC and AC saturation performances of PDs are closely related to electric field screening in the depletion region. By analyzing the electric field distribution under high optical injection levels, we can estimate the saturation characteristics of different PD structures. Furthermore, by adopting more accurate carrier transportation models, including velocity overshoot effect and thermal effect, it is possible to predict precisely the saturation current and 1-dB compression point.

In conclusion, a high-power and high-responsivity back-illuminated mesa-structure InGaAs-InP UTC-PD has been fabricated, and its saturation characteristics have been investigated. The device has demonstrated high responsivity and high RF output power. The responsivity is as high as 0.83 A/W at 1.55 μm. The device exhibits a 3-dB bandwidth of 9 GHz, and a RF

output power of 20.1 dBm has been recorded at the saturation photocurrent of 100 mA under a 6-V reverse bias. By taking into consideration the charge screening effect, the voltage drop over internal resistance and the voltage swing induced by AC current, the electric fields under different DC and AC injection levels have been calculated. The results reveal the dependence of the saturation performance on the complete field screening in the depletion region. Field screening analysis can be an efficient method for estimating the saturation characteristics of UTC-PDs in high power device design.

This work was supported by the National Basic Research Program of China (Nos. 2011CB301902 and 2011CB301903), the High Technology Research and Development Program of China (Nos. 2007AA05Z429 and 2008AA03A194), the National Natural Science Foundation of China (Nos. 60723002, 50706022, 60977022, and 51002085), the Beijing Natural Science Foundation (No. 4091001), and the Industry, Academia and Research Combining and Public Science and Technology Special Program of Shenzhen (No. 08CXY-14).

References

1. A. J. Seeds and K. J. Williams, IEEE J. Lightwave Technol. **24,** 4628 (2006).
2. T. Wang, Q. Chang, and Y. Su, Chin. Opt. Lett. **7,** 339 (2009).
3. T. Wang, H. Chen, S. Xie, B. Hraimel, L. Ma, and X. Zhang, Chin. Opt. Lett. **8,** 1037 (2010).
4. C. H. Cox III, E. I. Ackerman, G. E. Betts, and J. L. Prince, IEEE Trans. Microwave Theory Tech. **54,** 906 (2006).
5. J.-W. Shi, Y.-S. Wu, C.-Y. Wu, P.-H. Chiu, and C.-C. Hong, IEEE Photon. Technol. Lett. **17,** 1929 (2005).
6. Y. Huang, C. Huang, Q. Wang, H. Huang, X. Wang, and X. Ren, Chin. Opt. Lett. **3,** 53 (2005).
7. T. Ishibashi, N. Shimizu, S. Kodama, H. Ito, T. Nagatsuma, and T. Furuta, in *Proceedings of Ultrafast Electon. Optoelectron'97 Conference* 83 (1997).
8. N. Li, X. Li, S. Demiguel, X. Zheng, J. C. Campbell, D. A. Tulchinsky, K. J. Williams, T. D. Isshiki, G. S. Kinsey, and R. Sudharsansan, IEEE Photon. Technol. Lett. **16,** 864 (2004).
9. X. Li, N. Li, X. Zheng, S. Demiguel, J. C. Campbell, D. Tulchinsky, and K. J. Williams, IEEE Photon. Technol. Lett. **15,** 1276 (2003).
10. F. J. Effenberger and A. M. Joshi, IEEE J. Lightwave Technol. **14,** 1859 (1996).
11. J. Shi, F. Kuo, C. Wu, C. Chang, C. Liu, C. Chen, and J. Chyi, IEEE J. Quantum Electron. **46,** 80 (2010).
12. A. Beling, H. Pan, H. Chen, and J. Campbell, in *Proceedings of IEEE MTT-S Int.* 499 (2008).
13. K. J. Williams and R. D. Esmans, IEEE J. Lightwave Technol. **7,** 1443 (1999).
14. X. Wang, N. Duan, H. Chen, and J. Campbell, IEEE Photon. Technol. Lett. **19,** 1272 (2007).
15. N. Li, X. Li, S. Dimiguel, X. Zheng, J. Campbell, D. Tulchinsky, K. Williams, T. Isshiki, G. Kinsey, and R. Sudharsansan, IEEE Photon. Technol. Lett. **16,** 864 (2004).
16. C. Sun, J. Zhou, B. Xiong, J. Wang, and Y. Luo, Chin. Phys. Lett. **20,** 1312 (2003).
17. S. Demiguel, L. Giraudet, L. Joulaud, J. Decobert, F. Blache, V. Coupé, F. Jorge, P. Pagnod-Rossiaux, E. Boucherez, M. Achouche, and F. Devaux, IEEE J. Lightwave Technol. **20,** 2004 (2002).